RESEARCH ARTICLE

Symmetrical and Asymmetrical Breast Phantoms With 3D-Printed Anatomical Structure for Microwave Imaging of Breast Cancer

FATIMA-EZZAHRA ZERRAD[1], (Member, IEEE), **MOHAMED TAOUZARI**[2,3],
EL MOSTAFA MAKROUM[1], **SAROSH AHMAD**[4,5], (Graduate Student Member, IEEE),
FATIH Ö. ALKURT[6], **MUHARREM KARAASLAN**[6], **MD TARIKUL ISLAM**[7], (Member, IEEE),
AND MOUSA I. HUSSEIN[8], (Senior Member, IEEE)

[1]Laboratory IMII, Faculty of Sciences and Techniques, Hassan First University of Settat, Settat 26000, Morocco
[2]Laboratory LISA, National School of Applied Sciences, Hassan First University of Settat, Berrechid 26002, Morocco
[3]Aeronautical and Telecommunication Laboratory, International Academy of Civil Aviation, Casablanca 20040, Morocco
[4]Department of Signal Theory and Communications, Universidad Carlos III de Madrid, Leganés, 28911 Madrid, Spain
[5]Department of Electrical Engineering and Technology, Government College University Faisalabad (GCUF), Faisalabad 38000, Pakistan
[6]Electrical-Electronics Engineering, Iskenderun Technical University, 31200 Hatay, Turkey
[7]Department of Biomedical Engineering, University of Illinois at Chicago, Chicago, IL 60607, USA
[8]Department of Electrical Engineering, United Arab Emirates University, Al Ain 15551, United Arab Emirates

Corresponding authors: Sarosh Ahmad (saroshahmad@ieee.org) and Mousa I. Hussein (mihussein@uaeu.ac.ae)

ABSTRACT In this study, various breast phantom (BP) models for microwave breast imaging (MBI) are investigated and the creation and assessment of designed models are presented. Symmetrical and asymmetrical BP models have been constructed. based on 3D printed structures stuffed with various mixed material combinations that roles various breast tissue layers (skin, healthy fat tissue, glandular tissue, heterogeneous mix tissue, and tumor tissue) in terms of permittivity over the ultra-wide band frequency (3.1–10.6GHz) range. However, the main issue in making such phantoms is coming up with adequate material mixes that mimic those characteristics across the frequency band, as well as creating the phantom with realistic approach. The complex dielectric characteristics are tested after fabrication with a dielectric probe kit coupled to a VNA. Then, the measured complex dielectric properties are compared to the real human breast dielectric values. The symmetrical and asymmetrical phantoms' integrated structure allows the tumor and BPs to be dynamically combined to provide a test setup based on MBI technologies. Once the breast phantom has been produced, antenna arrays are positioned around it to collect scattering parameter data for tumor characterization. Finally, the extracted feature data was used to reconstruct the image in order to find the undesirable tumor component within the breast phantom using an imaging algorithm.

INDEX TERMS Microwave imaging (MWI), breast cancer detection, dielectric characterization, symmetrical and asymmetrical breast.

I. INTRODUCTION

Microwaves have a lot of interest in biomedical applications owing to their non-ionizing behavior, low cost, and portability [1], [2], [3]. Additionally, multiple investigations have demonstrated that, the dielectric characteristics of distinct human biological tissues differ significantly at the UWB

The associate editor coordinating the review of this manuscript and approving it for publication was Mira Naftaly.

frequency range [4], [5]. Therefore, in recent years, biomedical MWI, especially for breast tumor- cancer diagnosis, repels strong attention [6], [7], [8], [9]. The dielectric difference that may exist between a healthy tissues and malignant tissues is of particular interest in this type of utilization of microwave imaging. According to reference [10], the inconvenience ratio between malignant and benign adipose breast tissue layers 10. However, the percentage of those detected samples between tumors and normal fibroconnective–glandular tissues are less

than 10%, making MWI difficult to detect such cancers. In literature, there are many microwave imaging systems specialized to breast cancer detection [7] are currently undergoing clinical trials, despite the fact that microwave imaging is still a developing technique for medical imaging that is not yet accepted as a substitute for magnetic resonance imaging (MRI) or X-ray computed tomography (CT). However, before the clinical testing, the imaging systems must be evaluated by using reference anthropomorphic phantoms model to evaluate their performance in realistic environments. These reference BPs must meet the following criteria: Its structure must be like that of the human breast, and the dielectric characteristics of their constituent materials must be similar to those of the abovementioned portion's numerous biological tissues [11].

The construction of a novel symmetrical and most realistic asymmetrical phantoms with various diameters of tumors is presented in this work. The dielectric properties of each layer are measured, and a 3D printed shape with a complicated real human like structure is provided to make the phantom model more suitable in the MBI system experiments.

The following is a breakdown of how the paper is structured. The process utilized to make symmetrical and asymmetrical breast molds are described in Section 2. The production and characterization techniques for the various breast tissues are described in section 3 based on the literature findings. In Section 4, the measured dielectric parameters for each layer are shown, as well as a 3D shape with a detailed structure, that resembles a human breast, to make the phantom more suitable for MBI system experiments. The basic results of the asymmetrical breast phantom imaging with the MBI system are also explored in section 5. Finally, a conclusion section has been added to sum up the article.

II. 3D-PRINTED STRUCTURES
Utilization of breast phantoms in the evaluation of microwave imaging systems is critical. Diverse phantoms were created by various researchers [9]. Moreover, the development of extremely realistic breast phantoms has received high attention in recent years. A 3D printed breast phantom with an interior like the true fibro glandular tissue distribution obtained from the anatomy of a real human breast using CubePro Trio 3D Printer is demonstrated in this part. However, several types of 3D printing materials (filaments) have recently become available on the market. Two distinct types of: 3D-Prima Conductive ABS and PLA have been tested for dielectric and printing characteristics. The permittivity of the breast molds was measured using filament samples printed from the molds (as seen in the section 4). Both materials have values that are similar to those of air, according to the data. As a result, they are more ideal for incorporating dielectrically dense fabrics (gland tissue, tumors) that imitate liquids and materials, either by obviating the need for an additional non anatomical dielectric boundary layer or, at the least, by enhancing the transmission coefficient.

A. INTERIOR PHANTOM STRUCTURE
The breast phantom's anatomy was recreated using anatomical representations and CT scans [12]. The anatomy of the breast can be divided into four main primary structures, as shown in Figure 1, for the creation of a phantom: lactiferous ducts, and skin, mammary glands (fibro glandular tissue) and adipose tissues (fat) [13].

In most of the existing MBI systems on the market, the breast is in a direct contact with the system's surface. As a result, during measurement, the breast should correspond to the contour of the prototype. The experimental appraisal of conformal prototype, on the other hand, required the phantom models to have exact identical shape and anatomy of the real human breast. The authors create two sorts of BPs in this scenario: symmetrical and asymmetrical phantoms.
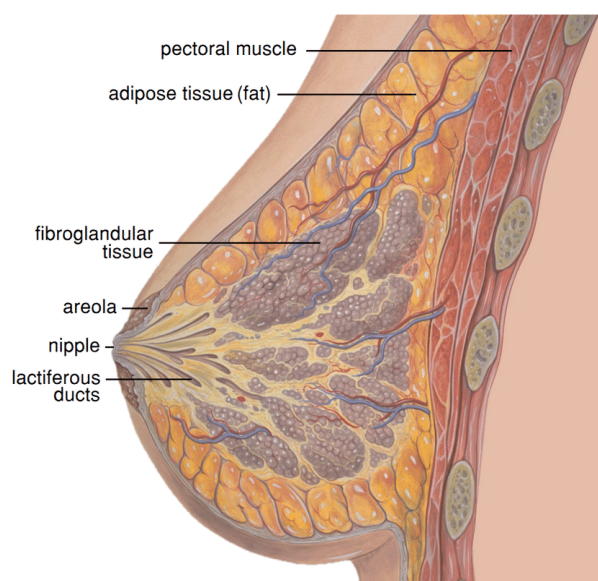

FIGURE 1. Breast anatomy - adapted from (https://commons.wikimedia.org/).

B. SYMMETRICAL BREAST PHANTOM STRUCTURE
The phantom is made up of four symmetrical chambers created by two inside 3D printed containers as illustrated in Figure 2. The BP is depicted in a schematic picture. A is for overview, B is for oblique view from above, C is for skin layer, D is for interior container, and a-d is for chambers.

The proposed 3-D mold enables for reproducing the breast anatomy's inter-individual diversity, particularly the fact that the proportion of fat tissue increases with age [14].

To begin with, a mixture that simulates adipose tissue can be used to fill the outer chamber (a), while adipose or mammary gland tissue imitation might be used to fill the gap between the inner and outer chambers (b). Moreover, the mixture with the electrical characteristics of breast mammary gland can be introduced in the interior chamber (c) and the mixture that presents the lactiferous ducts can be filled into the lower interior chamber (d). It will be filled from
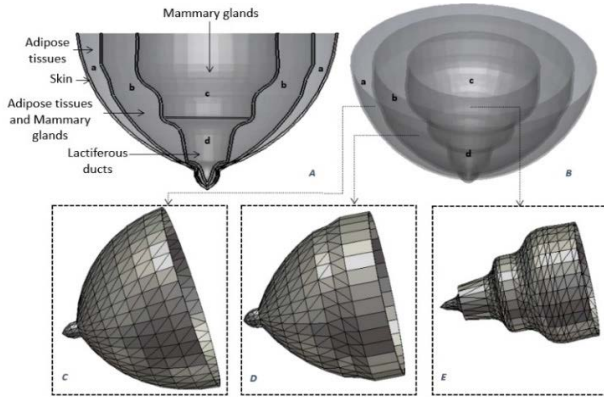
FIGURE 2. Symmetrical breast phantom mold. A overview, B view from above, C outer container, D interior container, E inner container.
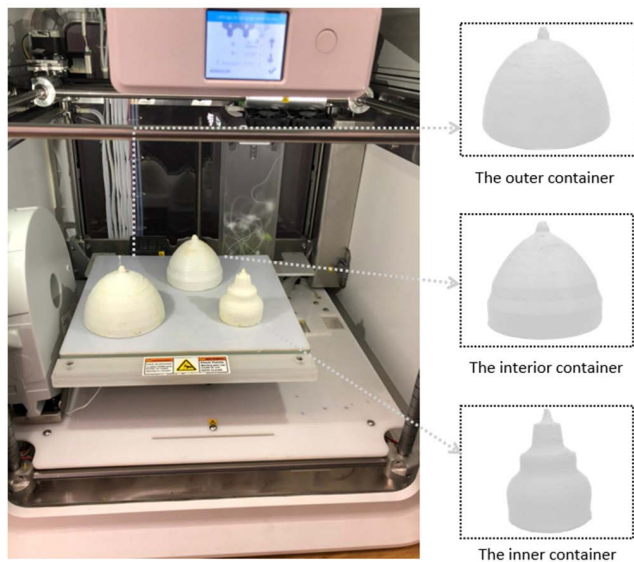

FIGURE 3. 3D printer with 3D printed symmetrical breast phantom containers.

above and separated with a 3D printed separator. Furthermore, different structures can be merged to present tumors, which can be 3D printed or another produced type, thanks to the employment of open-top configuration. It might be positioned in several locations to provide for the existence of a tumor.

However, the containers are 3D printed out of Proto-Pasta conductive (PLA) as shown in Figure 3.

C. ASYMMETRICAL BREAST PHANTOM STRUCTURE

The asymmetrical structure more accurately replicates the natural form of the anatomy, and it prevents the production of visual artifacts that are common in symmetrical structures. On the other hand, by using an asymmetrical phantom representing the inner breast anatomy, the poor performance of imaging algorithms that rely on symmetric phantom features could be easily "uncovered" [14]. The phantom is made up of four asymmetrical chambers created by two inside 3D printed

containers as shown in Figure 4. However, the containers are 3D printed out of Proto-Pasta conductive (PLA) as shown in Figure 5.
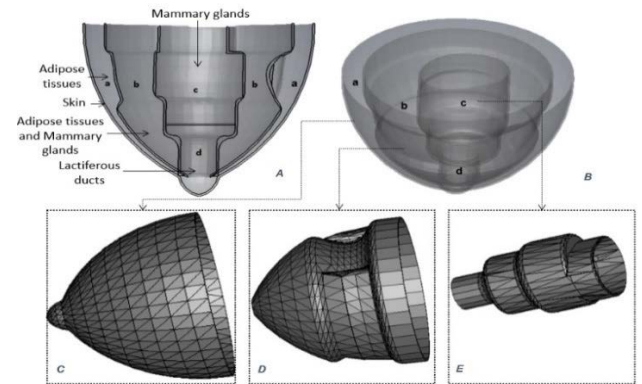

FIGURE 4. Asymmetrical breast phantom mold. A overview, B view from above, C outer container, D interior container.
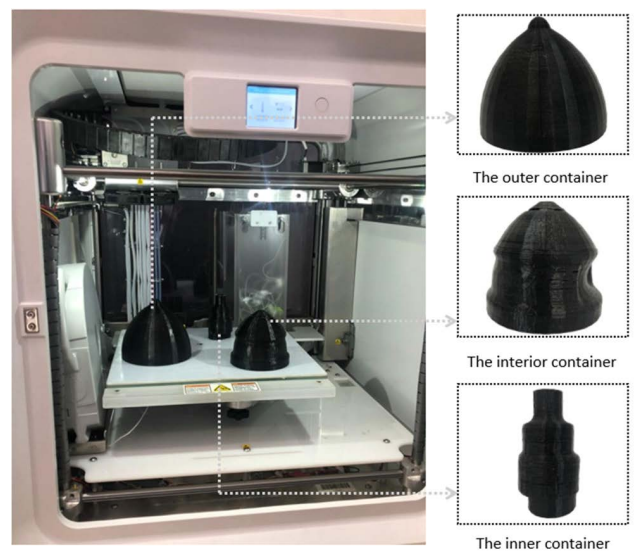

FIGURE 5. 3D printer with 3D printed asymmetrical breast phantom containers.

III. BREAST TISSUES DIELECTRIC FEATURES AND MANUFACTURING PROCURE

A. BREAST TISSUES LAYERS DIELECTRIC FEATURES

Table 1 lists the characteristics of a variety of breast phantoms that was described throughout the last decade. The phantoms' shapes and models can be simple geometrical shaped structures as homogeneous interior layers and more realistically shapes as heterogeneous interior layers. Designed breast phantoms are made of a variety of materials, ranging from dielectric characteristics that are near to those of breast tissue at specific frequencies to tissue mimicking materials [15] that perfectly approximate the dielectric properties of certain breast tissue throughout a wide frequency range. However,

TABLE 1. Review of previous research on bp for MWI applications.

Materials used for construction	Breast Form	ε_r, σ (S/m) of constituents					Fr (GHz)	Ref
		Skin	Fat	Gland	HMT	Tumor		
TX-100 NaCl	3D-printed structure		ε_r =4.76±0.04 σ = 0.18±0.03	ε_r =47±1 σ =1.61±0.08	ε_r =37.8±0.3 σ =1.12±0.05	ε_r =56±2 σ =1.79±0.06	2.45	[10]
Oil-in-gelatin	realistic	ε_r =34-21 σ =0.5-10	ε_r = 7.5-5.5 σ =0.01-1.8	ε_r =25-22.5 σ =0.5-10	-	ε_r =47.5-30 σ =0.5-15	0.05-13.51	[16]
Oil-in-gelatin	cylinder	ε_r =46-35 σ =12.5-18	ε_r =5-4.5 σ ≃1	ε_r =26-20 σ =2.5-5	-	ε_r =55-40 σ =15-21	0.5-8	[17]
TX-100 Salt	3D-printed structure	-	ε_r =4.7-5.2 σ =0.2-0.3	ε_r =46-49 σ =1.4-1.6	ε_r = 36-38 σ =1-1.14	ε_r =54-59 σ =1.72-1.85	2.45	[18]
Rubber solid	3D-printed structure	ε_r = 24 σ =1.6	ε_r =5 σ =0.2	ε_r =36 σ =3	-	ε_r >36 σ >3	3	[19]
ABS-Gelatine-Raisins	3D-printed structure	-	ε_r = 3.248 σ = 0.482	ε_r =48.7 σ = 5.504	-	ε_r =61.89 σ =16.21	8.5	[20]
Polyethylene	Hemi-sphere	ε_r = 22-40 σ = 1.5-2.5	ε_r = 5-15 σ = 1.7-2.5	ε_r = 15-45 σ = 1.5-4	-	ε_r = 35-56 σ = 3.5-8.5	3-10	[21]

TABLE 2. Composition of the bp.

| Material	Quantity					Purpose
	Skin	Fat	Gland	HMT	Tumor	
Sodium chloride (NaCl)	5g	4g	6g	4g	8g	Improve the conductivity
Distilled water	20ml	-	50ml	60ml	100ml	Increase the permittivity
Pure petroleum jelly	-	24g	-	-	-	Modify the permittivity
wheat flour	10mg	30g	30g	60g	-	Thickener, Modify the permittivity
Olive oil	-	30ml	-	-	-	Modify the permittivity
Powder dyes	(Orange)	(Green)	(Blue)	(Yellow)	(Dark Blue)	distinguish the different components
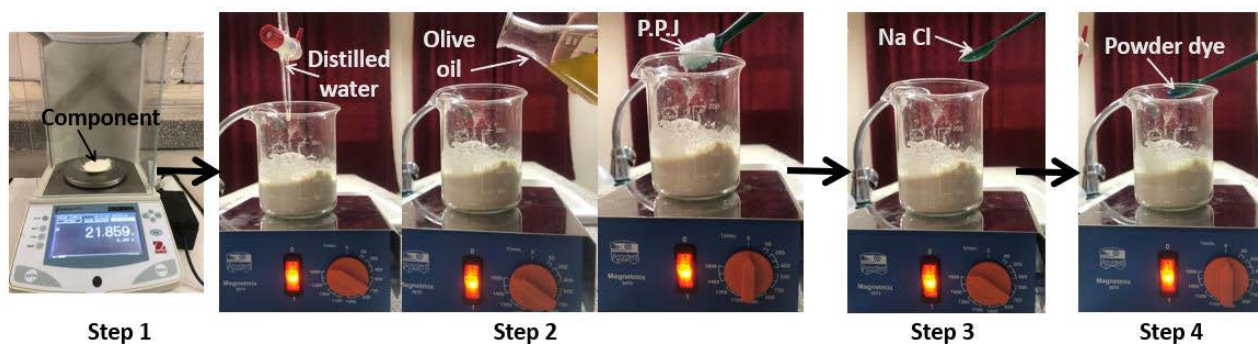
FIGURE 6. Representation of the breast phantom components preparation process.

Individual realistic breast phantom models that precisely replicate the shape, structural complexity, and microwave frequency dielectric characteristics of skin, fat, gland, heterogeneous mix tissue and tumor in the human breast are needed, which motivates our current research. For both symmetrical and asymmetrical phantoms, the features listed in [10] and [21] are still considered as most important properties of breast development.

B. FABRICATION PROTOCOL

To prepare each layer of the BP, the components and ratios are taken from Table 2. Fabrication and preparation of the different compositions of the breast phantom such as lactiferous ducts, skin, adipose tissues (fat), mammary glands (gland), Heterogeneous mix tissue (HMT) and tumor are made from various combinations of distilled water, wheat flour, pure petroleum jelly, olive oil, and Sodium Chloride (NaCl). The quantity is measured according to Table 2 (step1), and all steps are carried out at room temperature. The production method begins by adding gradually distilled water to wheat flour in a beaker to form a thick syrup (step 2). Due to its high dielectric characteristics over a wide frequency range (WFR), water is employed as a primary source of permittivity. However, stirring must be done slowly and carefully, rather than aggressively, as air bubbles might form and influence the dielectric characteristics. After that, NaCl is added in order to improve the conductivity of the mixtures (step3). This procedure with distilled water is applicable for fabricating heterogeneous mix tissue, skin and mammary glands. The oil is used alternatively for fabricating the adipose tissues (fat) in a same procedure with using pure petroleum jelly (P.P.J), since oil and P.P.J have low permittivity, which is ideal for decreasing the permittivity of phantom's fat. Finally, a small amount of different powder dyes was added to distinguish the different components of the breast (step4). Figure 6 shows the overall concepts for producing the phantom components. The materials utilized to fabricate the phantom components have excellent mechanical qualities, making it simple to construct the breast phantom by layering various components. The fabricated components are presented in Figure 7. In the next phase, the electrical properties of the produced components are validated.
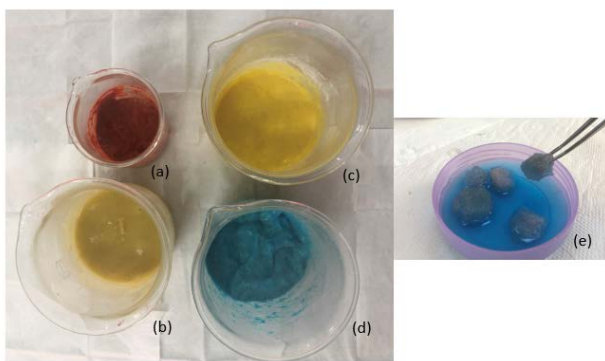

FIGURE 7. Fabricated components of the breast phantom (a) skin, (b) fat, (c) gland, (d) HMT and (e) tumor.

C. MEASUREMENT METHOD OF THE COMPLEX DIELECTRIC PROPERTIES

The measurements have been carried out up to 12 GHz since, this range between 2-12GHz includes that of many MBI studies in literature. In addition, this range provides to exactly compare the measurement results of the proposed breast parts presented in this study and the reference study. Besides this,

the frequency range of utilized antenna in MBI (4-10 GHz) fits with this investigated frequency range of breast layers in terms of electromagnetic properties.

The dielectric characteristics of the fabricated tissue-mimicking breast phantom are measured by using an Agilent PNA-L Vector Network Analyzer (VNA) and Agilent 85070E open-end coaxial linked probe kit. The Agilent 85070E dielectric probe kit includes a coaxial probe (see Figure 8(a)) could measure relative dielectric constants at frequencies ranging from 200 MHz to 20 GHz. This method is easy to use as non-destructive testing and could be used in both in-vivo and ex-vivo measurements over a WFR. The phase and amplitude of the reflected signal at the end of a coaxial probe inserted or submerged into solid, semi-solid, or liquid samples for measurement are used to determine the dielectric characteristics. In order to correct the post-calibration measurement, the VNA was initially calibrated using an open, short, and matched load prior to calibrating the open ended coaxial-line probe with measurements on air, a short circuit block, and distilled water.
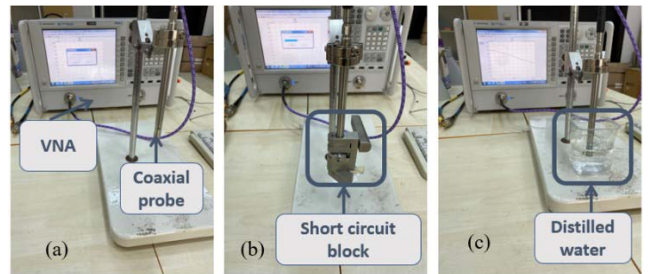

FIGURE 8. Measurement Setup: (a) Probe calibration with open circuit, (b) Probe calibration with short circuit block, and (c) Probe calibration with sterile water (Load).

The cross-section schematics of the employed coaxial probe with its electric field orientation are shown in fig. 9. The probe is made up of a shorter section of transmission line on which the EM waves propagate. The phase and amplitude of the reflected signals are generated when the probe and the targeted tissue sample have different impedances, which are then transformed into complex permittivity values by using the VNA. Different methods have been developed to convert the measured reflection coefficient to permittivity [22], [23], [24], [25]. The complex relative permittivity of a sample can thus be calculated from S11 using the bilinear equation shown below [25].

$$\varepsilon_r^* = \frac{C_1 S_{11} - C_2}{C_3 - S_{11}} \tag{1}$$

With complex calibration constants C_1, C_2, and C_3, calculated as follows:

$$C_1 = \frac{1 - S'_{22}}{j\omega Z_0 C_0(1 + S'_{22})} + \frac{C_f}{C_0} \tag{2}$$

$$C_2 = \frac{S'_{11} - S'_{11}S'_{22} + S'_{12}S'_{21}}{j\omega Z_0 C(1 + S'_{22})} + \frac{f(S'_{11} + S'_{11}S'_{22} - S'_{12}S'_{21})}{C_0(1 + S'_{22})} \tag{3}$$

$$C_3 = \frac{S'_{11} + S'_{11}S'_{22} - S'_{12}S'_{21}}{1 + S'_{22}} \qquad (4)$$

where C_f is capacitance determined by fringing-field effects inside the probe, C_0 is capacitance determined by fringing-field effects outside the probe tip that couple to the sample, and Z_0 is the coaxial transmission line's real characteristic impedance ($Z_0 = 50$).

However, today, this process is generally done automatically by software embedded in the VNA [26].

Figure 8(b)-(c) shows the initial calibration phase of the VNA and coaxial probe with sterile water and a short circuit block. After then, all the phantom samples are analyzed in the UWB frequency, and they are split independently to ensure that the probe has enough contact with the sample while taking measurements.

A visual examination of the inside half of each individual sample is performed to determine consistency. Moreover, to ensure that there is no space between the probe and the sample, the outer surface is designed as flat surface including sand (Figure 9).

Finally, five test data of each sample are taken at different positions throughout the surface for better accuracy and the mean value is then utilized to derive the final results. The phantom component measuring setup is depicted in figure 10. The measurement appears to be done as correctly as possible, with an average percentage error of less than 2%.

The probe kit presents data in terms of complex permittivity:

$$\varepsilon^* = \varepsilon_r - j\varepsilon'' \qquad (5)$$

where ε_r is the real component of permittivity (also referred to as the relative permittivity) and ε'' is the imaginary part of permittivity. The electrical conductivity, σ, is related to ε'' by the equation below:

$$\varepsilon'' = \frac{\sigma}{\omega\varepsilon_0} \qquad (6)$$

where ω is the frequency in radians and ε_0 denotes the free space permittivity.
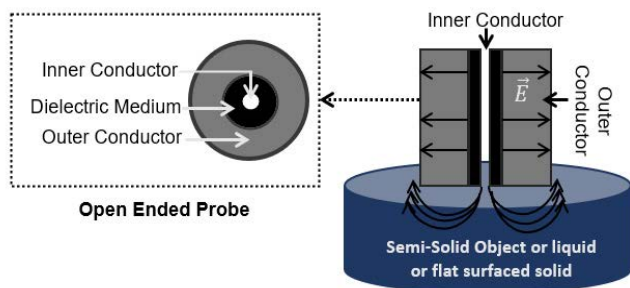

FIGURE 9. Schematics of the probe in cross-section with the electric field orientation.

IV. THE BP ELEMENTS' DIELECTRIC PROPERTIES

The produced BP components' dielectric characteristics are measured and compared to the reference relative

FIGURE 10. Measurement setup of the breast phantom components.

(Target) complex permittivity and conductivity, as shown in Figure 11.

Although the study covered the range of 2 to 12 GHz, we chose 3 GHz as a reference to compare our findings with those provided by [21]. Since the breast mold's shape is not flat, we measured data (permittivity and conductivity) from various BP mold corns to ensure that the mold's permittivity is low compared to the components of the breast phantoms and won't affect the results. However, there are also some errors in the measurement due to the accuracy and the temperature of the model; probe position; environmental parameter change; probe contamination; imperfect connection; cable movement, etc."

Nevertheless, for both symmetrical and asymmetrical phantoms, the features listed in [10] and [21] Table 1 are still considered the most important properties of breast development.

TABLE 3. Dielectric properties of the breast phantom.

Breast mold						
Properties	Data1	Data2	Data3	Data4	Data5	Mean
Permittivityε_r	0.9	1.12	1.15	1.6	1.75	1.3
Conductivity	0.02	0.02	0.03	0.03	0.04	0.03
Skin Layer						
Properties	Data1	Data2	Data3	Data4	Data5	Mean
Permittivityε_r	35.17	35.20	35.13	35.21	35.40	35.22
Conductivity	0.8	1.1	0.95	1.0	0.87	0.94
Fat Layer						
Properties	Data1	Data2	Data3	Data4	Data5	Mean
Permittivityε_r	4.86	4.88	4.90	5	5	4.92
Conductivity	0.2	0.15	0.17	0.18	0.18	0.17
Gland Layer						
Properties	Data1	Data2	Data3	Data4	Data5	Mean
Permittivityε_r	46.15	47	46.85	46.28	46.98	46.65
Conductivity	1.61	1.7	1.65	1.63	1.60	1.63
HMT Layer						
Properties	Data1	Data2	Data3	Data4	Data5	Mean
Permittivityε_r	37.12	37.51	37.77	37.81	37.63	37.56
Conductivity	1.12	1.17	1.10	1.16	1.14	1.13
Tumor						
Properties	Data1	Data2	Data3	Data4	Data5	Mean
Permittivityε_r	54.21	56.00	55.12	55.98	54.82	55.22
Conductivity	1.62	1.8	1.68	1.76	1.68	1.7

As a result, the relative dielectric permittivity of the skin, fat, gland, heterogeneous mix tissue (HMT) and tumor ranges

from 37–20, 5–3.6, 48–29, 38–21, and 56–36, respectively, as seen in the first measurement. The conductivity of the phantom components stated above ranges from 1.1–2.1, 0.1–1.0, 0.3–3, 1.2–2.6, and 1.25–4.7 (in S/m).
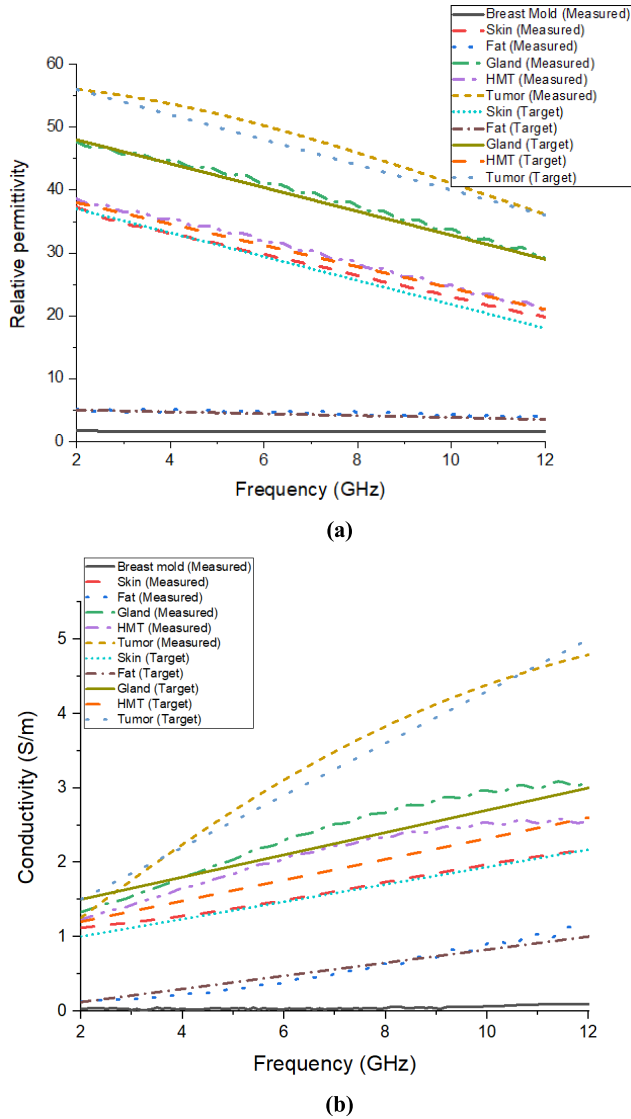

(a)

FIGURE 12. (a) Symmetrical and (b) asymmetrical fabricated breast phantom.

(b)

FIGURE 11. Dielectric properties of breast phantom: (a) measured and reference relative permittivity; (b) measured and reference conductivity against frequency.

However, to evaluate the effectiveness of the electrical properties of the breast phantom's components and to prove that the breast phantom is assumed to be homogeneous, the open-ended coaxial probe is placed at four more random locations. The deviation of measured electrical properties are in acceptable range Table 3 shows data from multiple positions of phantom components at frequency of 3 GHz, as well as their mean value.

As a result, the measured breast phantom model exhibits more realistic properties of real human breast tissue, allowing the electromagnetic breast imaging system to be evaluated. Figure 12 depicts the process of adding phantom components
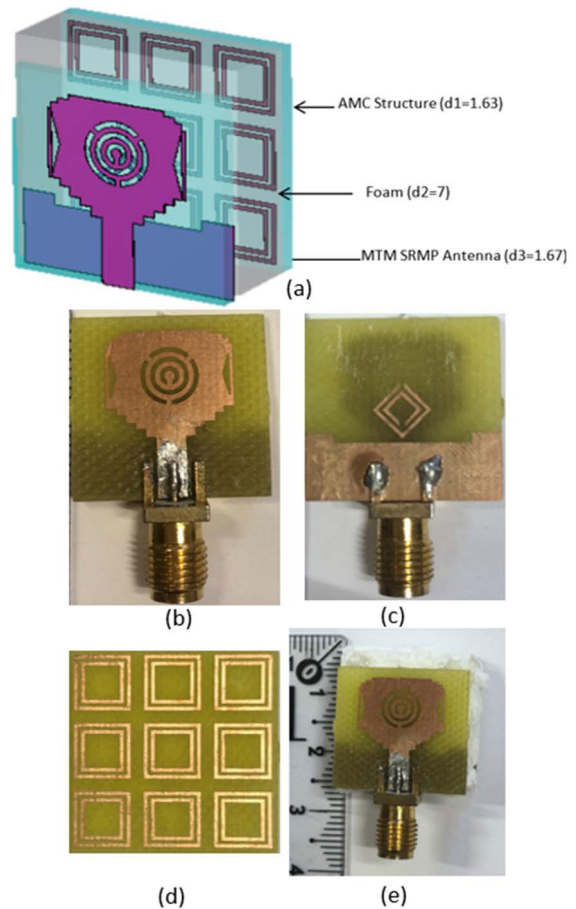

FIGURE 13. (a) The antenna design, and (b)-(e) the fabricated prototype. (The antenna parameters have been both simulated and measured.)

to a 3D breast mold. The skin is the first component to be inserted, followed by, fat, gland, heterogeneous mix tissue and tumor, respectively. Figure 12 shows how a 7 mm diameter straw was placed into the mold during the pouring process to create a hole for depositing the tumor material.
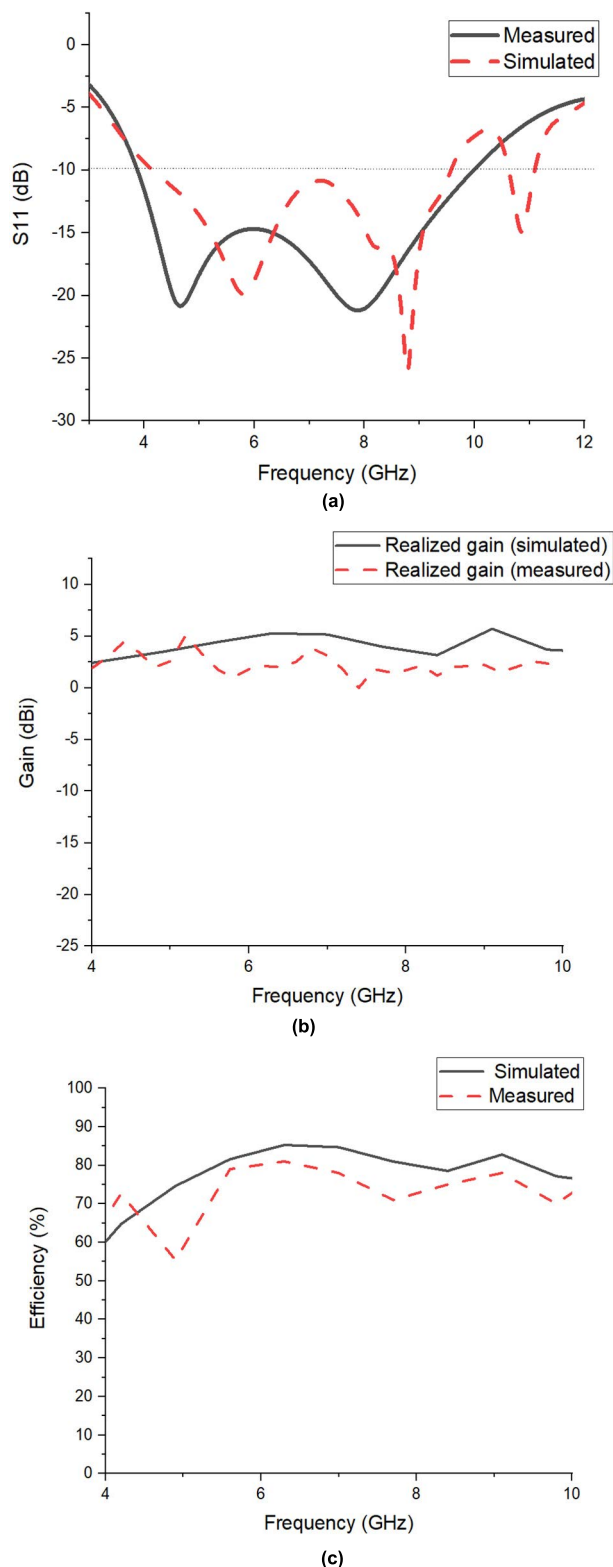
(a)

(b)

(c)

FIGURE 14. (a) S11, (b) the realized gain, and (c) the efficiency of the antenna.
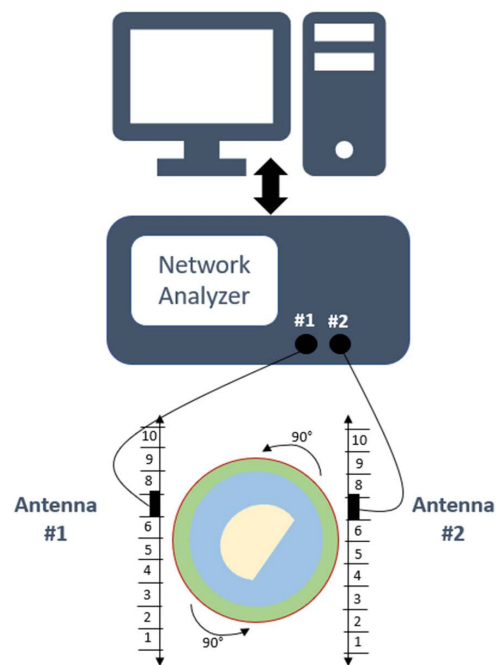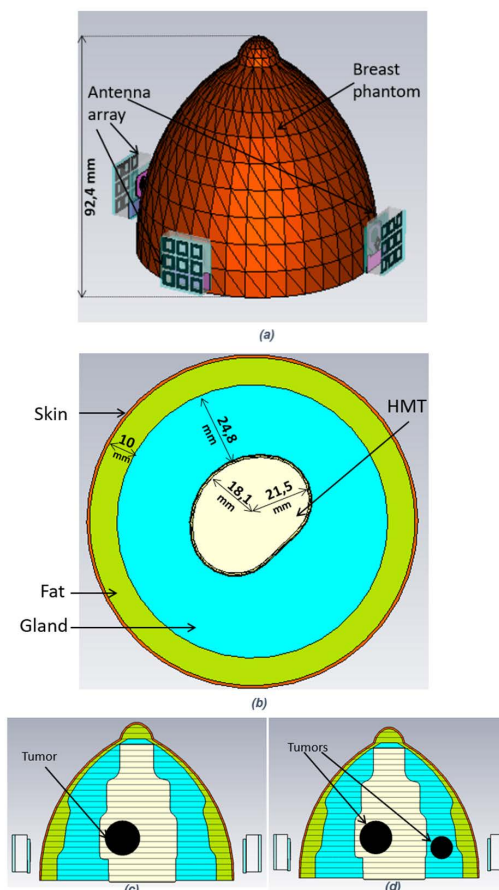

FIGURE 15. Proposed setup.

FIGURE 16. (a)-(b) Imaging system setup with asymmetrical breast, (c) Phantom with a tumor inside the phantom, and (d) phantom with two tumors.

V. SAMPLE IMAGES CREATED WITH MWI SYSTEM USING THE ASYMMETRICAL BREAST PHANTOM

This section examines sample images created from the MBI experiment configuration described at [27] with the proposed asymmetrical breast phantom, where backscattered signals are acquired using a microwave antenna

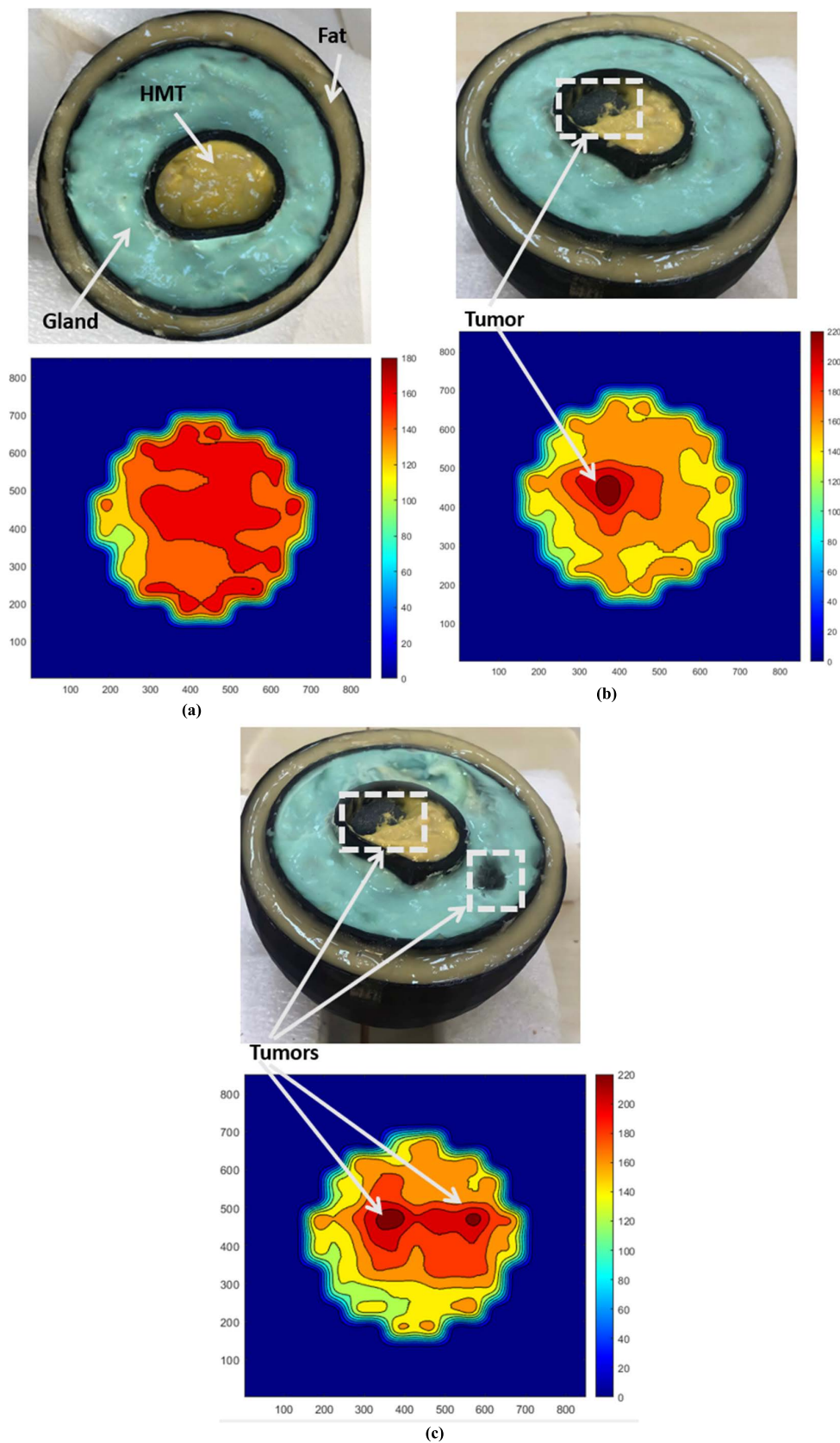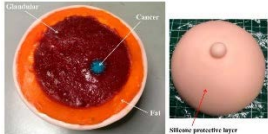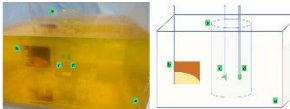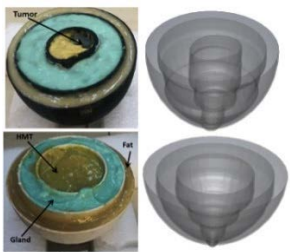**FIGURE 17.** Measured MWI results of the BP (a) BP without tumor, (b) BP with a tumor inside and (c) BP with two tumors.

TABLE 4. Comparison of produced tissue-mimicking breast phantoms with existing phantoms. Table 4 uses bold to emphasize the suggested analysis' attributes in comparison to existing literature.

Breast Phantoms	Breast shape	Fr	Tissues	Materials used for construction	Clear detection	ref
	Model of a hemispheric breast	2GHz-4GHz	-Skin -Fat -Glandular -Cancer (Tumor)	-Distilled water -Propylene glycol -Xanthan gum -200 Bloom calf-skin gelatin -Safflower Oil formalin (37% formaldehyde solution) -Surfactant	yes	[32]
	Cylinder made of styrene-acrylonitrile	1GHz-6GHz	-Low density breast tissue -Fibroglandular tissue -Tumor	-Styrene-acrylonitrile -Glycerin -TX151 -Water	yes	[28]
	Silicone rubber base	-	-Skin -Fatty tissue -Glandular	-Sorbitol -Sand -Liquid glycerin	yes	[29]
	Cylindrical with size of 3 inches	50 Hz - 50 MHz	-Skin layer -Fatty layer -Glandular layer -Transitional layer -Tumor	- Distilled water - Ctab -Safflower oil -Formalin -Propylene glycol -Gelatin -NaCl -Agar -Ethanol	yes	[30]
	Hemispherical with a radii of 60mm and 55 mm	3GHz-10GHz	-Skin -Fat -Gland (for heterogeneous Breast) -Tumor	-Distilled water -Safflower oil -Propylene glycol -Bloom calf-skin gelatin, -Formalin -Surfactant	yes	[31]
	Anthropomorphic (3D-printed structure and tissue-mimicking)	**2GHz-12GHz**	**-Skin** **-Fat** **-Gland** **- Heterogeneous mix tissue** **-Tumor**	**- NaCl** **-Distilled water** **-Pure petroleum jelly** **-wheat flour** **-Olive oil** **-Powder dyes**	**yes**	**Proposed**

sensor and images are constructed using a MATLAB script.

To start with, authors at [27] propose an UWB array antenna based on AMC structure. UWB is achieved by

introducing modified SRR into the patch as well as the ground as seen in figure 13. The antenna array was built and tested. The MTM AMC layout has been shown to enhance performance of the antenna, specially gain and directivity. The antenna has a higher BW of 7 GHz (4.1-9.7GHz), according to the findings in figure 14. Aside from that, a good radiation efficiency of even more than 85% is achieved, as well as a realized gain of 5.1 dBi. The antenna is a serious contender for MBI applications due to its compact size, high gain, and UWB capability.

Furthermore, the antenna fulfills excellently in both frequency and time domains. As shown in Figure 15, an experimental MBI was performed using the proposed BP and antennas. This configuration was used to collect the data.

Furthermore, scattering signals are produced by the interference of microwave signals from antennas and breast tissues. Antenna 1 emits and antenna 2 receives all backscattered and transmitted signals The transmission parameters are completely determined by the antenna path. The shallow depths beneath the skin layer are represented by the majority of the reflected parameters. The signals are bounced off to the opposite side of phantom and significantly attenuated. The reflected signals can be perfectly detected by an antenna with a higher gain and a lower reflection coefficient. The phantom was then displaced by 1 cm steps to achieve the best results with this MBI system. A board with 10 steps was marked appropriately between 0 and 10 cm and then deposited on a rotating table that rotated 90° to scan the breast on X and Y directions.

The Figure 16 shows the different setup of MWI system with asymmetrical breast phantom. Figure16(b) depicts a fabricated BP devoid of a tumor. Figure 16(c)-(d) shows the BP with a tumor inserted at a distance of 8 mm from the radius with a diameter of 10 mm, and the two tumors inserted in different locations, the second one at a distance of 24 mm from the radius with a diameter of 5 mm.

Additionally, a variety of data sets are obtained at 8GHz, including phantoms without tumors; phantoms with one tumor, and phantoms with two tumors. The antenna has the lowest measured loss coefficient and a high measured gain at 8GHz, allowing the MWI results to be used to predict the presence of small tumors. Figure 17 depicts all the sample images from the varying cases.

Figure 17(a) shows the image without the tumor and several lighter clutters due to the glandular tissue's significantly greater dielectric, but Figure 17 (b)-(c) clearly show the presence of one and two tumors, respectively. After examining the backscattering signals, the position and size of cancerous tissue cells were discovered to have a significant impact on the reconstructed images, which may be considered a systematic review of MBI systems.

VI. A COMPARISON OF THE FABRICATED BREAST PHANTOMS WITH EXISTING PHANTOMS

The produced tissue-mimicking BP and its abilities to detect cancer are compared to current developed breast phantoms

in Table 4. The suggested tissue mimicking BP including the most tissue parts is highly close to a real human breast according to the analysis tabulated in Table 4. On the one hand, the authors present the breast phantom in the form of a cylinder at [28], [29], [30]. The authors at [31], on the other hand, use a hemisphere mold and prepare the different tissue layers separately for molding, which takes more time. However, the use of the 3D printed breast phantom with an interior like the true fibro glandular tissue distribution obtained from the anatomy of a real human breast simplifies the fabrication process. Moreover, the building materials of the proposed BPs are accessible on the market at low cost and have excellent mechanical qualities, making it simple to construct the breast phantom by layering various components.

VII. CONCLUSION

Realistic phantoms are an innovative technique for determining the viability of new technologies, lowering the number of human and animal experiments in medical research, and optimizing design concepts that can be used to treat diseases. This work discusses the manufacture and measurement of medical breast phantom models. Two types of phantoms, symmetrical and asymmetrical with multiple layers of tissues, are produced separately, and a complex anatomy of a real human breast is constructed. These breast phantoms could be utilized to create a reliable and adaptable test platform for microwave tumor detection systems. The phantoms have five layers of skin, fat, gland, heterogeneous mix tissue and tumor that may be imaged using hemispheric conformal imaging systems.To validate the phantom qualities, the dielectric characteristics data are presented and compared to theoretical findings. The breast phantoms have a lifetime of one week after proper preservation in ambient air (T= 32°C) and longer in the refrigerator. Then, breast phantoms retain their properties for up to a week. As a result, the research described in this study has more realistic characteristics of an authentic human breast to test the breast cancer detection system's performance. Since, the proposed breast phantom models have the exact identical shape and anatomy of the real human breast, compared to the other works seen in [28], [29], and [30], where the authors used a cylindrical shape as a breast mold. Finally, sample images created with breast cancer detection systems from scanning of the proposed asymmetrical phantom in various settings (without and with tumors with high-resolution imaging) are also discussed.

REFERENCES

[1] Z. Xu, Y. Wang, and S. Fang, "Dielectric characterization of liquid mixtures using EIT-like transmission window," *IEEE Sensors J.*, vol. 21, no. 16, pp. 17859–17867, Aug. 2021, doi: 10.1109/JSEN.2021.3085954.

[2] E. Ghafar-Zadeh, M. Sawan, V. P. Chodavarapu, and T. Hosseini-Nia, "Bacteria growth monitoring through a differential CMOS capacitive sensor," *IEEE Trans. Biomed. Circuits Syst.*, vol. 4, no. 4, pp. 232–238, Aug. 2010, doi: 10.1109/TBCAS.2010.2048430.

[3] I. Vendik, O. Vendik, V. Pleskachev, I. Munina, P. Turalchuk, and V. Kirillov, "Wireless monitoring of biological objects at microwaves," *Electronics*, vol. 10, no. 11, p. 1288, May 2021, doi: 10.3390/electronics10111288.

[4] A. Peyman, B. Kos, M. Djokić, B. Trotovšek, C. Limbaeck-Stokin, G. Serša, and D. Miklavčič, "Variation in dielectric properties due to pathological changes in human liver," *Bioelectromagnetics*, vol. 36, no. 8, pp. 603–612, 2015, doi: 10.1002/bem.21939.

[5] J. Bourqui and E. C. Fear, "System for bulk dielectric permittivity estimation of breast tissues at microwave frequencies," *IEEE Trans. Microw. Theory Techn.*, vol. 64, no. 9, pp. 3001–3009, Sep. 2016, doi: 10.1109/TMTT.2016.2586486.

[6] F.-E. Zerrad, M. Taouzari, E. M. Makroum, J. Aoufi, H. Nasraoui, F. G. Aksoy, M. Karaaslan, and M. T. Islam, "Novel measurement technique to detect breast tumor based on the smallest form factor of UWB patch antenna," *Int. J. Microw. Wireless Technol.*, pp. 1–9, Mar. 2022, doi: 10.1017/S1759078722000289.

[7] D. O'Loughlin, M. O'Halloran, B. M. Moloney, M. Glavin, E. Jones, and M. A. Elahi, "Microwave breast imaging: Clinical advances and remaining challenges," *IEEE Trans. Biomed. Eng.*, vol. 65, no. 11, pp. 2580–2590, Nov. 2018, doi: 10.1109/TBME.2018.2809541.

[8] V. Khoshdel, M. Asefi, A. Ashraf, and J. LoVetri, "Full 3D microwave breast imaging using a deep-learning technique," *J. Imag.*, vol. 6, no. 8, p. 80, Aug. 2020, doi: 10.3390/JIMAGING6080080.

[9] M. Alibakhshikenari, "Metamaterial-inspired antenna array for application in microwave breast imaging systems for tumor detection," *IEEE Access*, vol. 8, pp. 174667–174678, 2020, doi: 10.1109/ACCESS.2020.3025672.

[10] N. Joachimowicz, B. Duchêne, C. Conessa, and O. Meyer, "Anthropomorphic breast and head phantoms for microwave imaging," *Diagnostics*, vol. 8, no. 4, p. 85, Dec. 2018, doi: 10.3390/diagnostics8040085.

[11] Y. Bao, H. Deng, X. Wang, H. Zuo, and C. Ma, "Development of a digital breast phantom for photoacoustic computed tomography," *Biomed. Opt. Exp.*, vol. 12, no. 3, p. 1391, Mar. 2021, doi: 10.1364/boe.416406.

[12] H. Zolfagharnasab, S. Bessa, S. Oliveira, P. Faria, J. Teixeira, J. Cardoso, and H. Oliveira, "A regression model for predicting shape deformation after breast conserving surgery," *Sensors*, vol. 18, no. 2, p. 167, Jan. 2018, doi: 10.3390/s18010167.

[13] A. C. Pelicano, M. C. T. Gonçalves, D. M. Godinho, T. Castela, M. L. Orvalho, N. A. M. Araújo, E. Porter, and R. C. Conceição, "Development of 3D MRI-based anatomically realistic models of breast tissues and tumours for microwave imaging diagnosis," *Sensors*, vol. 21, no. 24, p. 8265, Dec. 2021, doi: 10.3390/s21248265.

[14] B. Faenger, S. Ley, M. Helbig, J. Sachs, and I. Hilger, "Breast phantom with a conductive skin layer and conductive 3D-printed anatomical structures for microwave imaging," in *Proc. 11th Eur. Conf. Antennas Propag. (EUCAP)*, Mar. 2017, pp. 1065–1068, doi: 10.23919/EuCAP.2017.7928662.

[15] M. Lazebnik, E. L. Madsen, G. R. Frank, and S. C. Hagness, "Tissue-mimicking phantom materials for narrowband and ultrawideband microwave applications," *Phys. Med. Biol.*, vol. 50, no. 18, pp. 4245–4258, 2005, doi: 10.1088/0031-9155/50/18/001.

[16] J. Croteau, J. Sill, T. Williams, and E. Fear, "Phantoms for testing radar-based microwave breast imaging," in *Proc. 13th Int. Symp. Antenna Technol. Appl. Electromagn. Can. Radio Sci. Meeting*, Feb. 2009, pp. 1–4, doi: 10.1109/ANTEMURSI.2009.4805059.

[17] G. Worrell, X. Pan, Y. Kim, and B. He, "Minneapolis, Minnesota 2–6 September 2009," in *Proc. 31st Annu. Int. Conf. IEEE Eng. Med. Biol. Soc., Eng. Future Biomed.* Piscataway, NJ, USA, Sep. 2009, Art. no. 5332418.

[18] N. Joachimowicz, B. Duchêne, C. Conessa, and O. Meyer, "Easy-to-produce adjustable realistic breast phantoms for microwave imaging," in *Proc. 10th Eur. Conf. Antennas Propag.*, Apr. 2016, pp. 1–4.

[19] J. Garrett and E. Fear, "A new breast phantom with a durable skin layer for microwave breast imaging," *IEEE Trans. Antennas Propag.*, vol. 63, no. 4, pp. 1693–1700, Apr. 2015, doi: 10.1109/TAP.2015.2393854.

[20] V. Kumari, A. Ahmed, T. Kanumuri, C. Shakher, and G. Sheoran, "Early detection of cancerous tissues in human breast utilizing near field microwave holography," *Int. J. Imag. Syst. Technol.*, vol. 30, no. 2, pp. 391–400, Jun. 2020, doi: 10.1002/ima.22384.

[21] M. T. Islam, M. Samsuzzaman, S. Kibria, and M. T. Islam, "Experimental breast phantoms for estimation of breast tumor using microwave imaging systems," *IEEE Access*, vol. 6, pp. 78587–78597, 2018, doi: 10.1109/ACCESS.2018.2885087.

[22] D. K. Misra, "A quasi-static analysis of open-ended coaxial lines (short paper)," *IEEE Trans. Microw. Theory Techn.*, vol. MTT-35, no. 10, pp. 925–928, Oct. 1987, doi: 10.1109/TMTT.1987.1133782.

[23] T. W. Athey, M. A. Stuchly, and S. S. Stuchly, "Measurement of radio frequency permittivity of biological tissues with an open-ended coaxial line: Part I," *IEEE Trans. Microw. Theory Techn.*, vol. MTT-30, no. 1, pp. 82–86, Jan. 1982.

[24] J. P. Grant, R. N. Clarke, G. T. Symm, and N. M. Spyrou, "A critical study of the open-ended coaxial line sensor technique for RF and microwave complex permittivity measurements," *J. Phys. E, Sci. Instrum.*, vol. 22, no. 9, pp. 757–770, Sep. 1989, doi: 10.1088/0022-3735/22/9/015.

[25] Z. Chen, M. Schwing, J. Karlovšek, N. Wagner, and A. Scheuermann, "Broadband dielectric measurement methods for soft geomaterials: Coaxial transmission line cell and open-ended coaxial probe," *Int. J. Eng. Technol.*, vol. 6, no. 5, pp. 373–380, 2014, doi: 10.7763/ijet.2014.v6.728.

[26] *Keysight E5063A ENA Series Network Analyzer*, Keysight Technologies, Santa Clara, CA, USA, 2015.

[27] F.-E. Zerrad, M. Taouzari, E. M. Makroum, J. El Aoufi, M. T. Islam, V. Özkaner, Y. I. Abdulkarim, and M. Karaaslan, "Multilayered metamaterials array antenna based on artificial magnetic conductor's structure for the application diagnostic breast cancer detection with microwave imaging," *Med. Eng. Phys.*, vol. 99, Jan. 2022, Art. no. 103737, doi: 10.1016/j.medengphy.2021.103737.

[28] R. C. Conceição, H. Medeiros, D. M. Godinho, M. O'Halloran, D. Rodriguez-Herrera, D. Flores-Tapia, and S. Pistorius, "Classification of breast tumor models with a prototype microwave imaging system," *Med. Phys.*, vol. 47, no. 4, pp. 1860–1870, Apr. 2020, doi: 10.1002/mp.14064.

[29] D. Carvalho, A. J. Aragão, B. Sanches, H. D. Hernandez, and W. V. Noije, "Experimental evaluation of a software-defined radio through a breast phantom aiming at microwave medical imaging," *Microprocessors Microsyst.*, vol. 87, Nov. 2021, Art. no. 104381, doi: 10.1016/j.micpro.2021.104381.

[30] S. Poompavai and V. Gowri Sree, "Dielectric property measurement of breast—Tumor phantom model under pulsed electric field treatment," *IEEE Trans. Radiat. Plasma Med. Sci.*, vol. 2, no. 6, pp. 608–617, Nov. 2018, doi: 10.1109/TRPMS.2018.2868818.

[31] S. Kibria, M. Samsuzzaman, M. T. Islam, M. Z. Mahmud, N. Misran, and M. T. Islam, "Breast phantom imaging using iteratively corrected coherence factor delay and sum," *IEEE Access*, vol. 7, pp. 40822–40832, 2019, doi: 10.1109/ACCESS.2019.2906566.

[32] K. Hossain, T. Sabapathy, M. Jusoh, S.-H. Lee, K. S. A. Rahman, and M. R. Kamarudin, "Negative index metamaterial-based frequency-reconfigurable textile CPW antenna for microwave imaging of breast cancer," *Sensors*, vol. 22, no. 4, p. 1626, Feb. 2022, doi: 10.3390/s22041626.

FATIMA-EZZAHRA ZERRAD (Member, IEEE) was born in Morocco, in 1996. She received the engineer's degree in telecommunications and embedded systems from the Hassan First University of Settat (UH1), in 2019. She is currently pursuing the Ph.D. degree with the UH1. She is also a temporary Professor with the Department of Electrical, Electronic and Embedded Systems Engineering, UH1. She is also an Associate Researcher at the Aeronautical Telecommunications Laboratory, AIAC Casablanca, Morocco. Her main research interests include antenna design, wireless communication, RF engineering, and microwave imaging.

MOHAMED TAOUZARI is currently a Professor with the Laboratory LISA, National School of Applied Sciences, Berrechid, Morocco, and a Visiting Professor of the International Academy of Civil Aviation, Casablanca, Morocco. He has authored or coauthored a number of refereed journals, conference papers and a few book chapters on various topics with many inventory patents filed. His research interests include antenna design, RFID systems, and metamaterial antennas and filters.

EL MOSTAFA MAKROUM received the M.S. degree from the Mohammadia School of Engineering, University V Mohammed, Rabat, Morocco, in 2007, and the Ph.D. degree in computers and telecommunications from the Higher National School of Electricity and Mechanics, University Hassan II, Casablanca, Morocco. He is currently a Professor at the Faculty of the Sciences and Technology of Settat, Morocco. His current research interests include RFID antennas, propagation, and EMC problems.

SAROSH AHMAD (Graduate Student Member, IEEE) received the bachelor's degree in electrical engineering with specialization in telecommunication from the Department of Electrical Engineering and Technology, Government College University Faisalabad (GCUF), Pakistan, in 2021. He is currently pursuing the master's degree in advanced communication technology with the Department of Signal Theory and Communications, Universidad Carlos III de Madrid (UC3M), Madrid, Spain. He has published 17 conference articles, 35 high indexed international journals, and five book chapters by Springer. His research interests include antennas and propagations, rectennas for energy harvesting applications, bandpass filters, half- and full-wave filter antennas, active sensors, and the microwave imagining communication devices. He is a member of the IEEE Antennas and Propagation Society (APS). During his graduation, he received the fully funded PEEF Scholarship Award from the Prime Minister of Pakistan and the Silver Medal for his bachelor's program. During his volunteer-ship, he contributed himself as a Branch Treasurer at the IEEE GCUF, Faisalabad Subsection, for two years. After the graduation, he has received the fully funded Erasmus Grant Scholarship for his master's program in Madrid. During his graduation research period, he has participated in four international IEEE conferences over the world, where he has presented ten articles mostly in oral presentations. He has presented his two articles in the International Turkish Conferences, where he has received the Best Paper Award, one article in the International Moroccan Conference Proceedings and one article in IEEE EuCAP'22. He has served as a Volunteer for the 16th IEEE European Conferences on Antennas and Propagations. He has been selected for the fully funded MITACS Internship Program in the nationally ranked University of Canada called Carleton University, where he is working as a Researcher in the field of massive MIMO antennas.

FATIH Ö. ALKURT received the B.Sc. degree from Gaziantep University, Turkey, in 2016, and the M.Sc. degree from Iskenderun Technical University, Hatay, Turkey,.in 2019, where he is currently pursuing the Ph.D. degree. His research interests include antenna designs, microwave transmission lines, and metamaterials.

MUHARREM KARAASLAN received the Ph.D. degree from the Physics Department, University of Cukurova, Adana, Turkey, in 2009. He has authored more than 100 research articles and conference proceedings. His research interests include applications of metamaterials, analysis and synthesis of antennas, and waveguides.

MD TARIKUL ISLAM (Member, IEEE) was born in Bangladesh, in 1994. He received the B.Sc. degree in computer science and engineering from Patuakhali Science and Technology University (PSTU), in 2016, and the master's degree from the Department of Electrical, Electronic and Systems Engineering, Universiti Kebangsaan Malaysia (UKM), Malaysia, in 2020. He is currently pursuing the Ph.D. degree with the University of Illinois at Chicago (UIC), USA. He is also working as a Research Assistant at the Department of Biomedical Engineering, UIC. He has authored or coauthored a number of refereed journals and conference papers. His research interests include the photoacoustic and thermoacoustic imaging, wireless communication, and microwave imaging for cancer detection.

MOUSA I. HUSSEIN (Senior Member, IEEE) received the B.Sc. degree in electrical engineering from West Virginia Tech, Montgomery, WV, USA, in 1985, and the M.Sc. and Ph.D. degrees in electrical engineering from the University of Manitoba, Winnipeg, Canada, in 1992 and 1995, respectively. From 1995 to 1997, he was with the Research and Development Group, Integrated Engineering Software Inc., Winnipeg, working on developing EM specialized software based on the boundary element method. In 1997, he joined the Faculty of Engineering, Amman University, Amman, Jordan, as an Assistant Professor. He is currently a Professor with the Department of Electrical Engineering, United Arab Emirates University. He has over 100 publications in international journals and conferences. He has supervised several M.Sc. and Ph.D. students. His current research interests include computational electromagnetics, electromagnetic scattering, antenna analysis and design, metamaterial and applications, and material/bio-material characterization, and sensor design for bio applications.

• • •